Polymer Bulletin (2024) 81:4123–4148
https://doi.org/10.1007/s00289-023-04874-7

ORIGINAL PAPER

Incorporation of *Aloe vera* and green synthesized ZnO nanoparticles into the chitosan/PVA nanocomposite hydrogel for wound dressing application

Hosna Alvandi[1] · Hajar Rajati[1] · Tahereh Naseriyeh[1] · Seyyed Soheil Rahmatabadi[2] · Leila Hosseinzadeh[3] · Elham Arkan[1]

Received: 13 November 2022 / Revised: 13 April 2023 / Accepted: 28 May 2023 /
Published online: 8 July 2023

Abstract

Nanocomposite hydrogels including chitosan (CS)/polyvinyl alcohol (PVA)/*Aloe vera* (AV)/zinc oxide nanoparticles (ZnO-NPs) were prepared as a wound dressing. The ZnO-NPs was synthesized using green synthesis method by *Matricaria chamomilla* leaf extract. The hydrogels were investigated using ultraviolet–visible (UV–Vis), Fourier transform infrared spectroscopy, X-ray diffraction, and scanning electron microscopy (SEM). In addition, other properties such as mechanical properties, swelling ratio, degradation rate, water vapor transmission rate, porosity percentage, cell viability, and antibacterial efficacy of the hydrogels were assessed. The release of synthesized ZnO-Nps from hydrogels was investigated. The results show that the addition of 5 wt.% *Aloe vera* to CS/PVA, water absorption, and WVTR increased by 276% and 68.98%, respectively. The maximum tensile strength and Young's modulus were found for the CS/PVA/AV/ZnO hydrogel containing 2 wt.% NPs, increasing by 150% and 28% over CS/PVA hydrogel, respectively. The SEM images revealed the agglomeration of NPs by increasing the ZnO-NPs content, reducing the ZnO-NPs release and skin absorption. Also, the degradation rate decreases by increasing the ZnO-NPs content from 0.5 to 2 wt.%. The cell viability studies showed no toxicity after loading of ZnO-NPs into the hydrogel and showed proper antibacterial activity against *Staphylococcus aureus* and *Escherichia coli.*

Keywords Nanocomposite hydrogel · *Aloe vera* · Chitosan · ZnO nanoparticles · *Matricaria chamomilla* · Wound dressing

Extended author information available on the last page of the article

Introduction

Skin injuries mainly include burn wounds, tumors, abrasion, and chronic wounds. Auto grafts, allografts, creams, solutions, skin tissues engineering, and wound dressings are different tools for wound treatment strategies [1]. Among various wound care products, wound dressings are widely used because of their ability to heal wounds quickly and create a moist environment while acting as a barrier against bacterial transmission [2]. An extensive range of wound dressings is often used for different types of wounds and to target different stages of the wound healing process [3]. Since rapid and safe wound healing requires care of the desired level of moisture and proper gas circulation, it seems that hydrogels are the most promising materials for this purpose due to their ability to absorb secretions [4]. In addition, due to their similarity to living tissues in water content, soft and rubbery consistency, and little surface tension with water or any biological fluids, currently they are the widest group of chemical compounds used in the new generation of smart wound dressings [5–7]. Degradable hydrogels will be ideal for improving the existing bandages and developing a new and better drug delivery system.

Chitosan (CS) is a naturally occurring and partially acetylated polymer of chitin that contains reactive amino groups in its structure [8]. Among natural derivative polymers, CS is one of the most studied polymers as a hydrogel wound dressing due to its superior properties such as biodegradability, biocompatibility, adhesion, non-allergenicity, antibacterial activity, and reactivity [9]. The antibacterial activity of chitosan is ascribed to positively charged groups that can interact with negatively charged cell membrane components [10]. The central problem with CS and many other natural polymers is their low stability and mechanical strength during the treating of biomedical products. Therefore, blending a synthesized polymer such as poly (vinyl alcohol) (PVA) with CS, which is a natural polymer, has been considered as a solution to this problem to increase the stability of hydrogels in wound healing processes [11, 12].

PVA is a non-toxic, water-soluble, highly crystalline, biodegradable, and biocompatible polymer used widely as a hydrogel in wound dressing applications [13]. Blending CS with PVA may provide excellent properties for an ideal wound dressing, such as antibacterial properties, non-toxicity, and wound healing efficiency, as well as physical and mechanical stability.

The common methods for preparation of CS/PVA hydrogels are freeze thawing (FT), solution casting (SC) with thermal annealing, and phase separation (PS). Feiz et al. used PS technique with aqueous of $NaOH/Na_2SO_4$ solution as the coagulation medium for preparation of PVA hydrogel. They concluded that the PS technique causes the formation of high crystalline phases in the hydrogel structure, leading to a reduction of degradation rate with the ability to hold a high amount of moisture. In another study, PVA/CsMMT nanocomposite hydrogel membranes were successfully prepared for wound dressing by the phase separation method [14].

Recently, new attempts have been made to design composite hydrogels, like modifying with drugs of natural origin, mostly extracted from plants. Today, *Aloe*

vera (AV) is one of the most popular herbs in the world used widely in therapeutic applications, diet therapy, and modern medicine [15–17]. Since *Aloe vera* contains some pharmacological compounds including vitamins, sugars, enzymes, minerals, phenolic compounds, polysaccharides, and glycoproteins, it possesses many significant medicinal properties such as anti-inflammatory, antiseptic and antibacterial as well as the ability to improve the wound healing process. Furthermore, *Aloe vera* is associated with angiogenic properties that increase the formation of new blood vessels by increasing the secretion of vascular endothelial growth factors [18, 19]. Zinc oxide nanoparticles (ZnO-NPs) are the most popular materials used in wound dressing application due to their excellent characteristics such as high chemical stability [20], antibacterial and anti-inflammatory properties [21], as well as the release of Zn^{2+} ions in the vicinity of wounds causing rapid wound healing [21]. The antibacterial and wound healing properties of ZnO nanoparticles can be attributed to the photocatalytic abilities and the production of reactive oxygen species (ROS). It is worth mentioning that ZnO-NPs show a high level and excellent antibacterial activity because of the interaction of nanoparticles with the cell membrane and disturbing the electrical balance of the bacterial cell wall [22]. The mechanism of antibacterial effect of ZnO through disrupting the cell membrane has been reported as cell lysis by collapsing the cell walls of the cytoplasmic fluids inside the cells. Bacteria leak out and lead to cell death. Depending on the type of bacteria and the path of synthesis, the mechanisms may be different, that is, it causes changes and damage to cellular proteins and DNA and cell death [23].Various physical and chemical methods such as hydrothermal [24], microwave [25], sonochemical [26], electrochemical [25], photochemical [27], radiation [28], and chemical reduction methods [29] are used to synthesize nanoparticles. These methods require high energy consumption, high pressure, high operating costs, and toxic reagents. Therefore, green synthesis of nanoparticles using biological sources such as plants, bacteria, algae, and fungi has been considered as the most popular method by researchers [30, 31]. In the present study, ZnO nanoparticles were synthesized using the green synthesis method with *Matricaria chamomilla* extract and applied in three different concentrations in CS/PVA/*Aloe vera* hydrogel. To the best of the authors' knowledge, there is not any study available on the simultaneous addition of *Aloe vera* and ZnO-NPs to the CS/PVA blend hydrogel as a wound dressing. In fact, the aim of this study is to investigate: (a) the effect of addition of *Aloe vera* to CS/PVA blend on water adsorption capacity, water vapor permeability, morphology, antibacterial and mechanical properties of hydrogel and (b) the effect of addition of ZnO-NPs to CS/PVA/*Aloe vera* composite on the above-mentioned properties of the hydrogels. For this purpose, ZnO nanoparticles were synthesized using *Matricaria chamomilla* extract and the properties of nanoparticles were investigated using ultraviolet–visible (UV–Vis), Fourier transform infrared spectroscopy (FTIR), X-ray diffraction (XRD), and scanning electron microscopy (SEM). The nanocomposite hydrogels were prepared using phase separation method and characterized by water vapor transmission rate (WVTR), porosity, swelling, and degradation. Also, physical, morphological, mechanical, and antibacterial properties, and cell viability of hydrogels, as well as dermal adsorption of nanoparticles were investigated (Fig. 1).

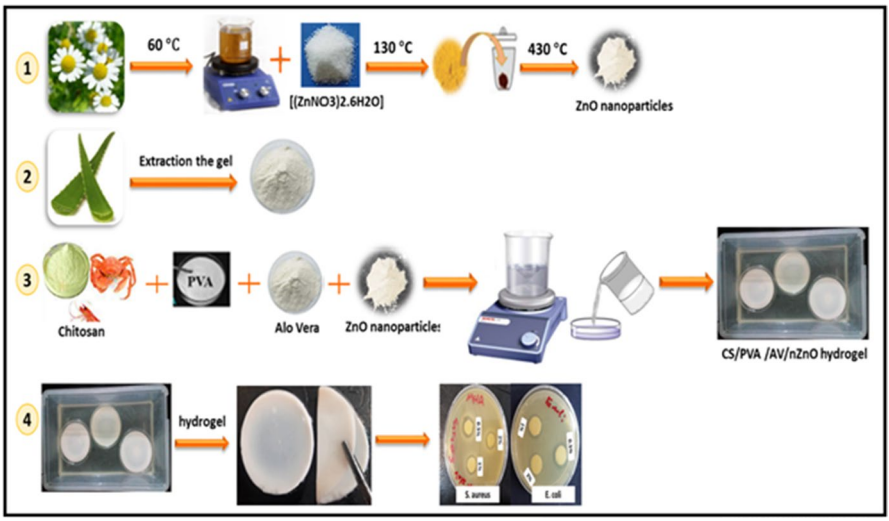

Fig. 1 A schematic preparation of nanocomposite hydrogels containing ZnO nanoparticles

Materials and methods

Materials

PVA (average $M_w = 72{,}000$ g/mol, 98% hydrolyzed) was purchased from Merck Co. (Germany). Chitosan ($M_w = 270{,}000$ g/mol, 85% degree of deacetylation) was supplied from Sigma-Aldrich Co. (USA). $Zn(NO_3)_2{\cdot}6H_2O$, sodium hydroxide (NaOH, 98% purity), sodium sulfate (Na_2SO_4, 99% purity), acetic acid ($C_2H_4O_2$, 99% purity), phosphate-buffered saline (PBS), and ethanol (C_2H_5OH, 98% purity) were also supplied by the Merck. Fresh plant *Matricaria chamomilla* and Fresh *Aloe vera* leaves were gained from the local market. Mouse fibroblast cells (L-929) were obtained from Pasteur Institute of Iran. *Staphylococcus aureus* (*S. aureus*) and *Escherichia coli* (*E. coli*) strains were obtained from Royan Institute of Iran.

Preparation of plant extract

To prepare the aqueous extract of *Matricaria chamomilla*, the flowers of this plant were washed several times with distilled water to remove all dust particles and other impurities from the plant surface. The flowers were dried in the shade to remove moisture and then ground. 5gr of plant powder was added to the beaker containing 100 mL of distilled water at 60–70 °C and stirred for 30 min. The mixture was kept for 1 h at room temperature to cool down and then filtered with Whatman filter paper No. 1 [32]. The extract was stored in the refrigerator for further use as a reducing, stabilizing, and inhibiting agent to synthesis ZnO nanoparticles.

Green synthesis of ZnO nanoparticles

To synthesis ZnO nanoparticles, 50 mL of *Matricaria chamomilla* extract was placed on a magnetic stirrer at 60–80 °C. Then, 5 g of zinc nitrate was added to *Matricaria chamomilla* extract under a magnetic stirrer at a constant speed of 150 rpm at 80 °C. After the reaction was completed, the solution was allowed to stand overnight and then the supernatant was discarded. The resulting precipitate was dried at 130 °C in an oven. Afterward, the resulting light yellow precipitate was grinned with a ceramic mortar to obtain a uniform powder. Finally, it was heat-treated for 3 h at 430 °C. After cooling down to room temperature, the zinc oxide nanoparticles (ZnO-NPs) were obtained as a pale white powder.

Preparation of Aloe vera powder

The *Aloe vera* powder was prepared by fresh leaves [33]. Briefly, the leaves were washed with distilled water and their green skin was carefully separated from the inner gel. The parenchyma was homogenized by mechanical mixer and then centrifuged at 10,000 rpm for 30 min. The resulting mucilage was lyophilized with a freeze dryer (Alpha 2–4 LD Plus, Martin Christ, Germany) and the dried powder was stored at 4 °C.

Preparation of hydrogel membranes

The hydrogels of CS/PVA, CS/PVA/AV(5, 10, and 15 wt.%), and CS/PVA/AV(5%) at three different ZnO-NPs loadings (0.5, 1, and 2 wt.%) were prepared through phase separation method [14]. Firstly, a solution of 2% (W/V) chitosan in 1% acetic acid at room temperature and a solution of 8% (W/V) PVA in distilled water at 70 °C were prepared separately. The two solutions were mixed as CS/PVA in a ratio of 3:1 for 6 h using a magnetic stirrer to obtain a homogeneous polymer solution. *Aloe vera* with three different ratios of 5, 10, and 15% (W/W) (relative to the CS/PVA total weight) were added to the CS/PVA solution and stirred overnight to obtain a uniform mixture. Then, ZnO nanoparticles with ratios of 0.5, 1, and 2% (W/W) (relative to the CS/PVA total weight) were suspended in 5 mL of ethanol/distilled water at a ratio of 50/50 and sonicated for 30 min. Afterward, the ZnO-NPs suspension was added to the CS/PVA/AV solution. The prepared solutions were cast into clean Petri dishes and then were put in an oven at 55 °C for 15 min to remove some extent of the solvent. Subsequently, the Petri dishes were immersed in the aqueous solution of NaOH (1 N)/Na_2SO_4 (saturated) as a coagulation media for 12 h. The obtained hydrogel membranes were washed several times with distilled water and dried in a freeze dryer at − 80 °C for 24 h to perform swelling and degradation tests and other analyses.

Characterization techniques

The wavelength of ZnO nanoparticles was determined by a UV–Vis spectrometer (UV-1650 PC, Shimadzu, Kyoto, Japan) in the wavelength range of 200–600 nm.

An X-ray diffractometer (PW1730, 40 kV, 40 mA, Philips, Netherlands) was used to identify the phases and crystallinity of ZnO-NPs. The source used was Cu Kα radiations ($\lambda = 1.54$ Å) with 2θ range from 20° to 80°. The size of crystals can be calculated according to the Scherrer equation:

$$D = k\lambda/\beta \cos\theta \tag{1}$$

where D is the mean size of the crystals (nm); λ is X-ray wavelength (1.54 Å); k is Scherrer constant (0.9 radians); β is full width at half maximum (FWHM) in radians, and θ indicates the diffraction angle [34].

The chemical structure of ZnO nanoparticles and prepared hydrogels was analyzed using FTIR spectroscopy (Shimadzu 8101 M FTIR, Kyoto, Japan). Each spectrum was acquired from 128 scans in the wave range of 4000–400 cm^{-1} with a resolution of 4 cm^{-1}. The morphological properties of ZnO nanoparticles were investigated using field emission scanning electron microscopy (FE-SEM, ZEISS-model Sigma VP, German). The size range of zinc oxide nanoparticles was calculated using Image J software (National Institutes of Health, free-trial version, USA). The average size of ZnO-NPs was obtained by measurement of at least 100 randomly selected nanoparticles. The morphology of the hydrogels was investigated using scanning electron microscope (SEM, TESCAN-VEGA3 SB, Brno, Czech Republic). The elemental atomic composition analysis of hydrogel membranes was conducted using SEM by energy-dispersive X-ray spectroscopy (EDX) and qualitative and quantitative analyses were conducted on samples.

The mechanical properties of the prepared hydrogels were assessed using a tensile testing machine based on ASTM D882-02 standard (Santam STM-1). The hydrogels were cut into 4 cm × 1 cm pieces (with 0.3 cm thickness) and then put into the apparatus. The test was performed two times for each sample with a speed of 5 mm/min at room temperature.

Porosity

To calculate the porosity of hydrogels, the samples were immersed into ethanol to reach the saturation state. The porosity was calculated from the following equation:

$$P(\%) = \frac{(V1 - V3)}{(V2 - V3)} \times 100 \tag{2}$$

Briefly, hydrogel of weight W was immersed in a graduated cylinder containing ethanol.

The volume of ethanol ($V1$), and the volume of hydrogel and ethanol was recorded as $V2$. After one hour, the samples were removed, and the volume of ethanol remaining was recorded as $V3$.

Swelling studies

To measure the swelling ratio of the samples, the hydrogels were cut into square specimens (2 cm × 2 cm) and placed in a vacuum oven at 60 °C for 24 h to dry completely. Then, the samples were weighed and placed in 15 mL PBS solution (pH = 7.4) at 37 °C. Samples were gently removed from the buffer solution at various intervals and were dried with filter paper. Then, the samples were weighed and returned to the same container. This process was continued until the sample weight reach to a constant value. The swelling ratio (S) was measured using the following equation:

$$S(\%) = \frac{w_1 - w_0}{w_0} \times 100 \tag{3}$$

where w_1 is the weight of the swollen hydrogel membrane and w_0 is the initial weight of the dry hydrogel membrane [34]. Three replicates for each model were done to obtain the mean value.

Weight loss analysis

The weight loss of the hydrogels was measured according to the classical gravimetric method [35, 36]. An appropriate amount of dry hydrogels (w_0) was immersed in PBS at 37 °C and then taken out of the container at various intervals (1, 3, 7 days). They were dried in a vacuum oven overnight at 60 °C and then weighted again (w_1). The test was conducted three times for each sample and then the weight loss of hydrogel was calculated using the following equation:

$$\text{Weight Loss}\,(\%) = \frac{w_0 - w_1}{w_1} \times 100 \tag{4}$$

Water vapor transmission rate (WVTR)

WVTR was calculated according to the European Pharmacopoeia (EP) standard [23, 37]. Briefly, the hydrogel sample was cut into a circular shape with a thickness of 3 mm and a diameter of 35 mm and was placed on the opening of a bottle with an inner diameter of 34 mm containing 25 mL of distilled water and secured with Teflon tape. The bottles were weighed and then placed in an incubator with constant temperature (37 °C) and relative humidity of 35% (Irankhodsaz, IKH-RH, Iran). The bottles were removed after 24 h and weighed again. WVTR was obtained from the following equation:

$$\text{WVTR}\left(\frac{\text{g}}{\text{m}^2\text{day}}\right) = \frac{\left(W_\text{i} - W_\text{f}\right)}{A} \tag{5}$$

where A is the permeation area of the samples, and W_i and W_f are the initial and final weight of bottles, respectively.

In vitro dermal adsorption study

The diffusion of ZnO-NPs from nanocomposite hydrogels was investigated by the dermal adsorption method from rat skin to evaluate the passage of zinc oxide nanoparticles. The Sprague Dawley rats with the weight range of 150–200 g were used for this study. All the animals were kept in the same conditions before the experiment. Storage conditions included polycarbonate cages, uniform food and water, and 12-h light–dark periods. The animals were anesthetized with chloroform and then killed. The entire abdomen of the animal was thoroughly dissected. The skin of this area was completely removed. Then, the fat under the skin was thoroughly removed and kept in normal saline solution until use. To be closer to the body conditions and to prevent changes in the physicochemical and biological properties of the skin due to long-term storage, the skin was freshly prepared at each time. To investigate the release of ZnO-NPs from nanocomposite hydrogels and dermal absorption, the French diffusion cell was used as a two-compartment model. The cell was filled with 30 mL of phosphate buffer (pH = 7.4) as the receptor phase. To approximate the body condition, the temperature of the diffusion cell was kept constant at 37 °C. Sampling was performed at different times (0.5, 2, 4, 6, 8, 10, 12, 24, 36, and 48 h). To establish equilibrium conditions, an equal amount of fresh buffer solution was replaced after each sampling. The experiments were performed in triplicate. The amount of ZnO-NPs adsorption passing through the rat skin was determined in samples using UV–Vis analysis.

Cell viability analysis

Toxicity of synthesized hydrogels of CS/PVA/AV and CS/PVA/AV/ZnO was measured by MTT assay (3-(4,5 dimethylthiazol-2-yl)-2,5-diphenyltetrazolium bromide, Sigma Co., St. Louis, Mo, USA). The test was conducted based on the viability of mouse fibroblast cells (L-929) according to ISO 10993–5 standard. Before performing the test, to prohibit cell death due to existence of any microbial contamination, the hydrogels were sterilized by exposing each side of samples to UV rays for 20 min. The mouse fibroblast cells were seeded in a 24-well plate (1×10^5 cells/well) and cultured at 37 °C in a humidified incubator with 5% CO_2 for 48 h and then incubated with MTT reagent (0.5 mg/mL in PBS) for 3 h. Afterward, the cells were washed with PBS to remove non-reacted MTT and then the formazan crystals were dissolved in the isopropanol solvent. Finally, the samples were investigated by an optical microscope at the wavelength of 570 nm with a spectrophotometric plate reader (Multiskan FC, Thermo Scientific) to evaluate cell viability. All the experiments were carried out in triplicate. The cell viability was calculated by dividing the absorption rate of each sample into control sample.

Antimicrobial activity evaluation

Antibacterial activity of prepared hydrogels against *S. aureus* and *E. coli* was determined by disk diffusion method using Mueller–Hinton Agar (MHA) medium. Agar plates were prepared by dissolving 38 g of the medium in the 1 L of distilled water and then autoclaved. Afterward, the solution was poured into the plate and let to solidify. Thereafter, 100 µL of prepared bacterial suspension (10^8 CFU/mL) was spread on an agar plate and then the samples were cut into circles of 2 cm diameter, placed on the agar plate, and then incubated at 37 °C for 24 h. The inhibition zone around each hydrogel sample without any bacterial growth was measured and considered as the antibacterial property of ZnO-NPs.

Results and discussion

Characterization of ZnO-NPs

UV–visible spectrophotometer analysis

Zinc ion reduction was investigated using a UV spectrophotometer in the range of 200–600 nm. The wavelength change is attributed to the plasmonic resonance of the product surface, which in turn is determined by the size and nature of the particles [38, 39]. The maximum wavelength observed in the UV–Vis spectrum of ZnO-NPs was at 369 nm (Fig. 2a). Awwad et al. synthesized zinc oxide nanoparticles (ZnO-NPs) using *Ailanthus altissima* extract and observed a similar peak at 369 nm in UV–Vis spectrum of ZnO nanoparticles [40].

FTIR spectroscopic analysis

FTIR spectroscopy was performed to identify functional groups in the ZnO-NPs sample. Due to interatomic vibrations, metal oxides generally form adsorption bands in the fingerprint region below 1000 cm^{-1} [41]. Figure 2b depicts the FTIR diagram identifying the functional group of ZnO nanoparticles obtained by the green synthesis method. The peak at 430 cm^{-1} is characteristic vibration of the ZnO-NPs. The broad band appeared at about 3415 cm^{-1} is attributed to the stretching vibrations of the OH groups in $Zn(OH)_2$ or the water molecule absorbed on the surface of ZnO crystals. The bands at 1382 cm^{-1} and 1495 cm^{-1} are related to the bending vibrations of OH and HOH groups, respectively [41, 42].

X-ray diffraction analysis

Figure 2c shows the XRD pattern of the obtained ZnO nanoparticles. The main diffraction peaks are appeared at 2θ equal to 31.9, 34.2, 36.2, 48.9, 57.1, 63.9, 67.3, 68.8, 69.6, 73.3, and 77.3° indexed as (100), (002), (101), (102), (110), (103), (200), (112), (201), (004), and (202) planes. The results are similar with those of ZnO powder obtained from the International Center of Diffraction Data card

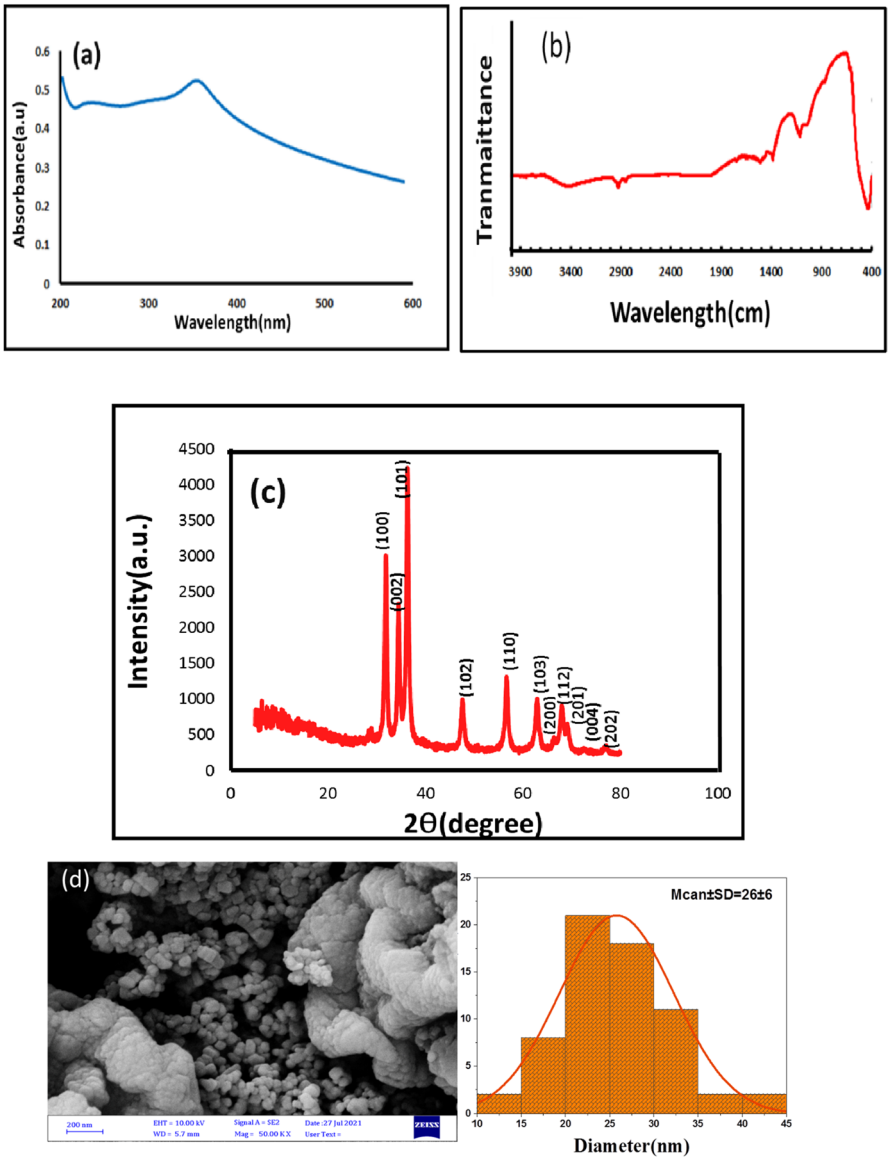

Fig. 2 **a** UV–Vis spectrum, **b** FTIR spectrum, **c** XRD pattern, **d** FE-SEM image and particle size distribution of the produced ZnO-NPs

(JCPDS-36-1451) confirming the formation of a crystalline monoclinic structure [43]. No extra diffraction peaks of other phases are detected, indicating the phase purity of ZnO-NPs [40, 41]. The average crystallite size of the synthesized nanoparticles (D) was calculated using the Scherrer formula (Eq. 1), which was obtained as 24 nm.

FE-SEM analysis

Figure 2d shows the FE-SEM image of the ZnO-NPs and the diagram of size distribution of these nanoparticles. Nanoparticles show a spherical shape with a dense structure. The nanoparticle size distribution was obtained from FE-SEM image and using Image J software (National Institutes of Health, free-trial version, USA), with considering 100 nanoparticles, randomly. The results demonstrated that the size range of ZnO-NPs, synthesized in the current study, was between 10 and 45 nm, and the average size of nanoparticles was calculated as 26 nm.

Characterization of hydrogel membranes

Appearance of hydrogel membranes

Each of chitosan and polyvinyl alcohol polymers was prepared by phase separation method alone. Both polymers had the ability to transform into hydrogels in the coagulant solution and were different from each other in terms of mechanical properties. Preparation of hydrogels by combining polymers in coagulation solution improved the mechanical properties compared to hydrogels prepared from individual polymers.

Figure 3 depicts the appearance of the prepared hydrogel membranes. As can be seen, the hydrogels show proper flexibility, homogeneous structures, and relatively uniform thicknesses. After visual and tactile inspection, it was observed that hydrogels with a higher content of AV (10 and 15 wt.%) are more fragile than that of 5 wt.% AV content. These results were consistent with a report by Bialik et al. [44]. Therefore, the CS/PVA/AV hydrogel with 5% AV content was selected to prepare nanocomposite hydrogels. It was observed that by the addition of ZnO-NPs in three different content (0.5, 1, and 2 wt.%) to CS/PVA/AV (5%) hydrogel, not only cracks

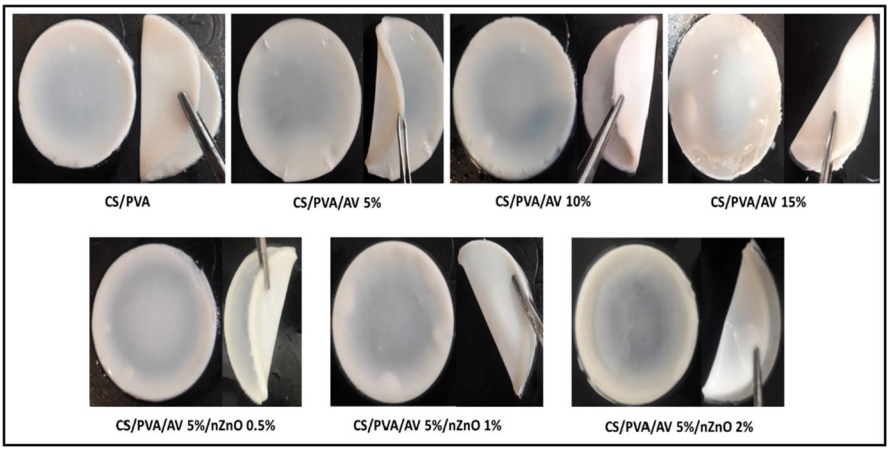

Fig. 3 The physical appearance of hydrogels

and fractures were removed from the hydrogel structure, but also it became more flexible.

FTIR spectroscopy analysis

Figure 4 shows the FTIR spectra of AV, ZnO-NPs, PVA, CS, CS/PVA, CS/PVA/AV, CS/PVA/AV/ZnO (0.5%), CS/PVA/AV/ZnO (1%), and CS/PVA/AV (2%).

Aloe vera showed a broad absorption band at about 3398 cm^{-1} related to amine (-NH) groups. The absorption bands at 2881 and 2922 cm^{-1} are due to the

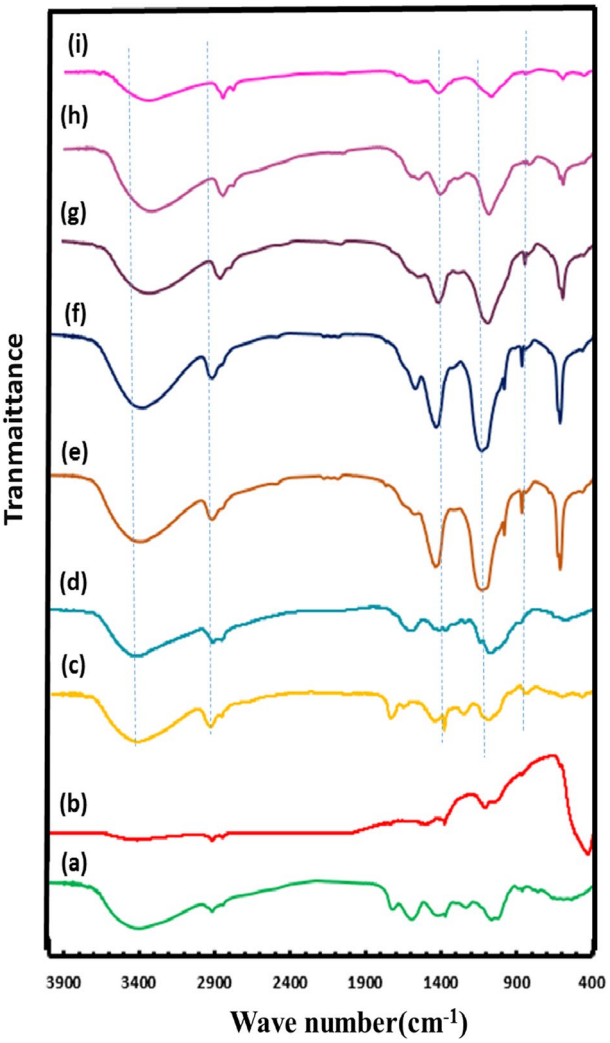

Fig. 4 FTIR spectra of **a** AV, **b** ZnO-NPs, **c** PVA, **d** CS, **e** CS/PVA, **f** CS/PVA/AV (5%) hydrogels, and CS/PVA/AV (5%) nanocomposite hydrogel containing **g** 0.5%, **h** 1%, and **i** 2% ZnO

symmetric and asymmetric stretching vibration of the $–CH_2$ groups, respectively. The absorption band at 1720 cm^{-1} indicated the presence of carbonyl groups (C = O). The strong absorption band at 1598 cm^{-1} is related to the C = C stretching vibration of vinyl ether. The absorption band at 1236 cm^{-1} is assigned to the stretching vibrations of the C-O groups of esters and phenols (Fig. 4a) [33, 45]. The FTIR spectrum of synthesized ZnO-NPs shows in Fig. 4b. The band appeared at 430 cm^{-1} is the characteristic of ZnO nanoparticles. Figure 4c depicts the FTIR spectrum of pure PVA, showing a broad absorption peak at 3387 cm^{-1} related to hydroxyl groups (O–H). The peaks at 2845 and 2920 cm^{-1} are associated with the symmetric and asymmetric stretching vibrations of C–H bonds. The peak related to the C-O bond is appeared at 1086 cm^{-1}. The FTIR spectrum of the neat chitosan hydrogel (Fig. 4d) shows a broad absorption band at 3441 cm^{-1} attributed to the overlapping of the stretching vibrations of amine groups (-NH) and hydroxyl groups (-OH). The characteristic peaks of the bending vibrations of amine and amide groups observe at about 1598 cm^{-1} and 1680 cm^{-1}, respectively. The peaks at 896 cm^{-1} and 1155 cm^{-1} are assigned to the saccharide structure of the chitosan [46]. The spectrum of PVA/CS hydrogels (Fig. 4e) indicates that the amine bending vibrations of chitosan shift toward lower wavelength (from 1598 cm^{-1} to 1440), due to the formation of a strong hydrogen bonding between $–NH_2$ of chitosan and –OH of PVA [47].

Generally, when two or more polymers are blended, the physical and chemical interactions between their molecules cause some changes in the characteristic peaks of their pure spectra. These observations demonstrate that there is good miscibility between CS and PVA. Based on the analysis of the FTIR spectrum after modification of hydrogel with *Aloe vera*, it can be concluded that the presence of additives does not have a direct effect on the chemical structure of the compounds. However, the CS/PVA/AV spectrum (Fig. 4f) shows some changes in the intensity and position of the peaks due to the presence of some interactions between chemical bonds. These changes especially can be seen at the range wave number of 3000–3500 cm^{-1} and 1200–1579 cm^{-1} due to the presence of many active substances, including polysaccharides [44]. As seen in CS/PVA/AV/ZnO spectrums (Fig. 4g–i), the different vibrational states of FTIR peaks are similar in nanocomposites and pure components with small chemical changes. With increasing ZnO-NPs percentage, the intensity of peaks shows a significant decrease.

SEM analysis of the hydrogels

The shape and morphology of the hydrogels were analyzed by scanning electron microscopy. One of the essential properties of the hydrogels is the porosity of the dressing matrix, as a large amount of porosity will be applicable for transporting nutrients and oxygen through the bandage. In addition, the porous nature is applied for absorbing large amounts of exudate from the wound surface and reducing infection [48]. As seen in Fig. 5, all the prepared hydrogels show a porous structure.

The SEM images of the cross section of CS/PVA hydrogel (Fig. 5a) show a uniform structure with micron-size pores without any cracks or phase separation, confirming good compatibility between PVA and CS polymer matrices [49]. As can be seen in CS/PVA/AV SEM images (Fig. 5b), the addition of AV to the CS/PVA blend

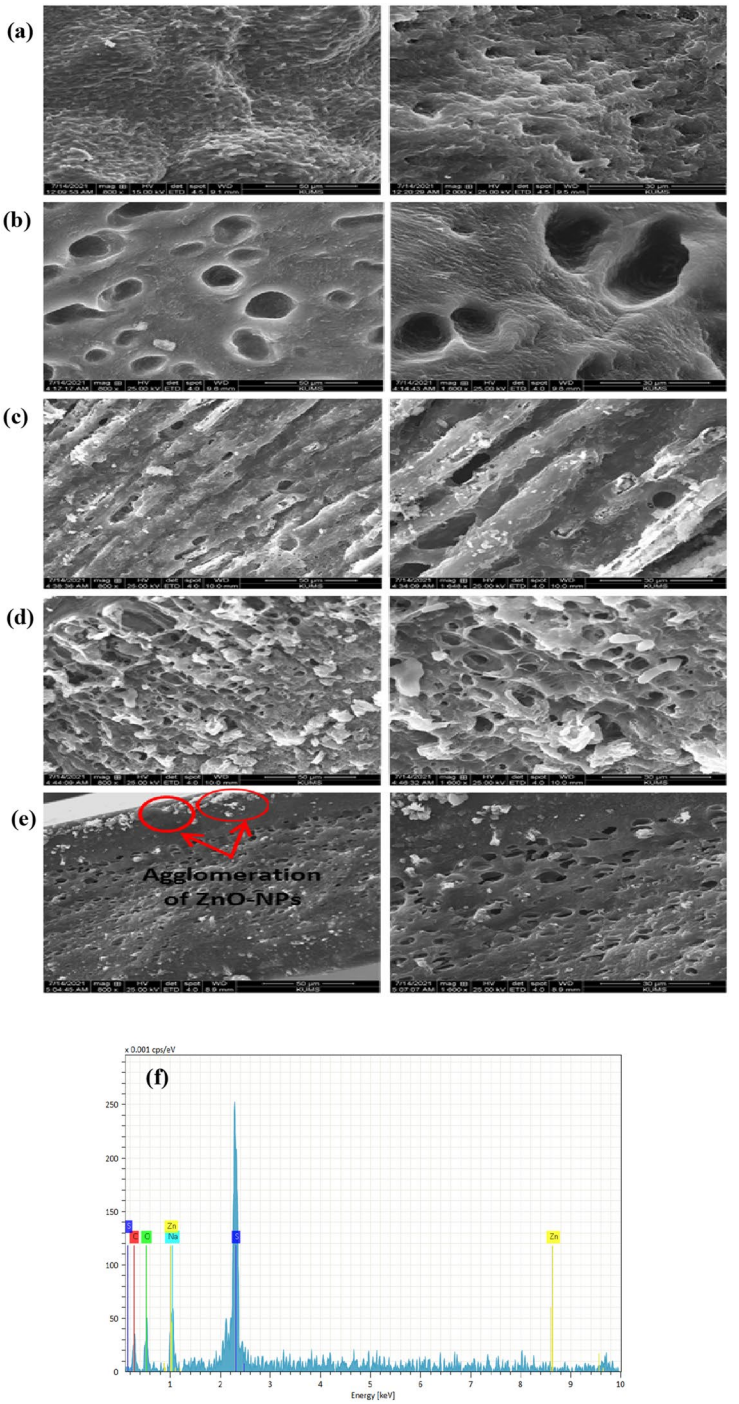

Fig. 5 SEM images of the cross section of **a** CS/PVA, **b** CS/PVA/AV, **c** CS/PVA/AV/ZnO (0.5%), **d** CS/PVA/AV/ZnO (1%), **e** CS/PVA/AV/ZnO (2%), and **f** EDX of ZnO-NPs in hydrogel matrix

leads to an increase in the porosity of the hydrogel. Jithendra et al. [45] also reported a similar result for addition of AV to collagen/chitosan hydrogel. SEM images of the CS/PVA/AV/ZnO (0.5%) hydrogel (Fig. 5c) show a more uniform morphology compared to those free from ZnO-NPs. From Fig. 5c, it is obvious that the nanoparticles are dispersed uniformly in the hydrogel matrix and reduce the hydrogel pore size. Also, stretches and fiber grooves were appeared in the SEM micrograph of the CS/PVA/AV/ZnO (0.5%) hydrogel as shown in Fig. 5c. This morphology could improve the hydrogel tensile properties that will be discussed in Mechanical strength section. For CS/PVA/AV/ZnO (0.5%) hydrogel, it is supposed that the presence of ZnO-NPs could improve the compatibility of two polymers via creating a proper mixing, so the hydrogel shows a more uniform morphology. It should be noted that chitosan has a strong ability to form metal complexes with zinc metal due to the presence of amine groups and hydroxyl groups in its structure that can interact with ZnO-NPs [50]. Furthermore, the hydroxyl (OH) groups of PVA have a great propensity to form a charge–transfer complex with ZnO-NPs via chelation. These strong interactions decrease the chain mobility of the polymer matrix and consequently the free volume and porosity of the CS/PVA/AV/ZnO (0.5%) hydrogel reduce. In fact, the strong affinity between CS, PVA, and ZnO-NPs makes the hydrogel structure denser.

As seen in Fig. 5d, e, increasing the ZnO-NPs content leads to a significant increase in the hydrogel porosity, which may be due to the poor interaction between polymer matrix and nanoparticles at higher concentration of ZnO-NPs. The poor interaction between two phases (polymers and ZnO-NPs) leads to the presence of some voids in the polymer/filler interphase, increasing the hydrogel porosity. As shown in Fig. 5e, with 2 wt.% incorporation of ZnO-NPs, particle agglomeration occurs in some regions, especially at the surface of the hydrogel membrane. It seems that in this case, the ZnO-NPs tend to agglomerate due to the disability of the polymer chains to cover all of the single particles.

EDX analysis was used to identify zinc atoms and ZnO-NPs distribution in the nanocomposite hydrogel with 2 wt.% ZnO-NPs loading. The elemental distribution EDX map for the CS/PVA/AV/ZnO (2%) nanocomposite hydrogel is shown in Fig. 5f. According to the EDS results, the synthesized zinc oxide contains Zn, Na, O, C, and S elements, which indicates the presence of chamomile extract on the synthesized nanoparticles.

Mechanical strength

The wound dressing hydrogel must have adequate mechanical properties including tensile strength and modulus elasticity. The effect of addition of AV and ZnO-NPs on the mechanical properties of the wet hydrogels was investigated by using tensile tests and the results are listed in Table 1. The results in Table 1 show that the tensile strength (σ) and elongation at break (ε) for the CS/PVA hydrogel increase with the addition of 5 wt.% AV while the Young's modulus (E) of this sample decrease. This observation may be due to the higher porosity of the CS/PVA/AV hydrogel leading to higher water absorption compare to the CS/PVA, based on the SEM analysis (see Fig. 5). The increase in water content of the hydrogel led to an increase in the plasticization effect of the adsorbed water into the polymer matrix. It was cussed

Table 1 Mechanical properties of hydrogel membranes

Hydrogel	Tensile strength (MPa)	Young's modulus (MPa)	Elongation at break (%)
CS/PVA	0.092 ± 0.006	0.69 ± 0.0014	19.21 ± 0.62
CS/PVA/AV	0.147 ± 0.024	0.47 ± 0.0017	63.70 ± 1.74
CS/PVA/AV/ZnO (0.5%)	0.03 ± 0.005	0.73 ± 0.0007	5.55 ± 0.60
CS/PVA/AV/ZnO (1%)	0.080 ± 0.004	0.82 ± 0.0008	11.48 ± 0.70
CS/PVA/AV/ZnO (2%)	0.215 ± 0.048	1.55 ± 0.0016	13.81 ± 0.64

enhancement of the σ and ε [33]. The desirable properties of wound dressings depend on where they are applied. If they are applied for highly mobile limbs (the elbow, knee, etc.), stretching of the dressing is preferred; otherwise, keeping such a dressing will be difficult. In other cases, a stiffer dressing is preferred [51]. In the current study, it is demonstrated that by addition of the proper amount of ZnO-NPs, the mechanical property of such a dressing can be adjusted depending on where it is used.

As seen in Table 1, the addition of 0.5 wt.% content of ZnO-NPs to the CS/PVA/AV hydrogel decreases the σ and ε by 74.3% and 83.6%, respectively, while increases E by 5.8% compared to the CS/PVA/AV hydrogel. Further increase in ZnO-NPs content leads to a significant increment in the value of σ, E, and ε, while the maximum tensile strength and Young's modulus were obtained for the hydrogel with 2 wt.% ZnO-NPs (150% and 28% increase in σ and E compared to the CS/PVA hydrogel, respectively).

Based on the SEM analysis, the addition of 0.5 wt.% ZnO-NPs to the CS/PVA/AV hydrogel causes a decrease in the porosity of the hydrogel membrane leading to reduction of the adsorbed water. So the plasticization effect of the adsorbed water decreases and the sample becomes more brittle, resulting in an increment in Young's modulus and a reduction in the σ and ε. As seen in Table 1, adding more ZnO-NPs content increases the tensile strength, elongation at break, and Young's modulus of the samples. Increasing the value of σ, E, and ε with the addition of more ZnO-NPs indicates that the nanoparticles act as reinforcing filler in hydrogel membrane, providing a more rigid/stiff behavior [51]. Although nanoparticle agglomeration was seen in the SEM images of the hydrogel with 2 wt.% ZnO-NPs, it seems that the plasticization effect of the adsorbed water on improving mechanical properties is more than the agglomeration of ZnO-NPs due to the large porosity of the CS/PVA/AV/ZnO(2%) hydrogel absorbing a great amount of water (Fig. 5e).

Swelling studies

Swelling of the hydrogel membrane due to its water holding capacity plays an important role in its antibacterial activity, wound healing, and medical applications. Hydrogels can absorb a small to moderate amount of wound exudate by swelling, which helps the wound to heal quickly. The swelling results of the hydrogel depend on the nature of the polymer network, include the presence of hydrophilic groups,

cross-link density, polymer network stretch, pH, and temperature of the swelling environment. Thus, any variation in the structure of the hydrogel network directly affects its swelling behavior [52]. According to the swelling study, the hydrogels absorbed water very quickly and reached a swelling equilibrium (a constant value of weight) after 3 h of immersion in PBS. Generally, the cause of water uptake of the CS/PVA hydrogels may be the porous structure of them, PVA hydroxyl groups, and chitosan amino groups, which interact with hydrogen molecules via H-bonding.

Figure 6 shows the water absorption profiles of the hydrogels, when immersed into PBS at 37 °C. Figure 6a shows that addition of 5 wt.% content of *Aloe vera* to the CS/PVA hydrogel increases the swelling ratio (water absorption) compared to CS/PVA sample. It is expected that the addition of *Aloe vera* disturbs the polymer networks and increases the free volume of the CS/PVA polymer blend, leading

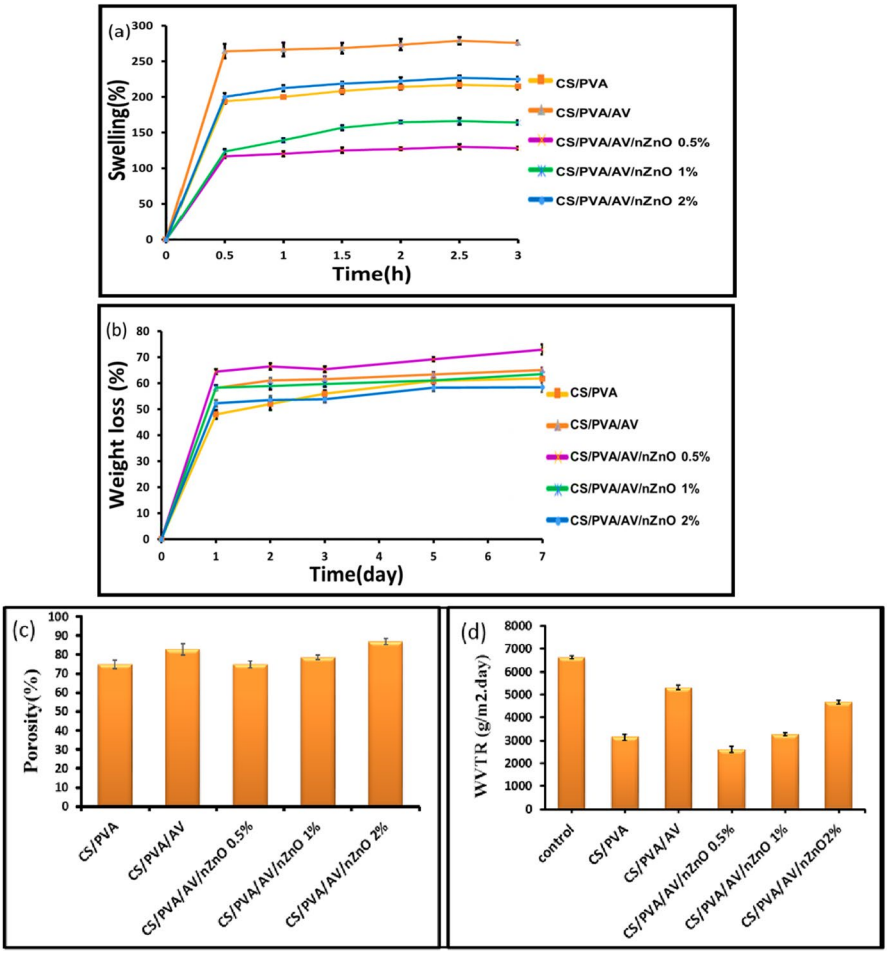

Fig. 6 Swelling (%) (**a**), weight loss (%) (**b**), porosity (**c**), WVTR (**d**) hydrogel membranes

to an increase in polymer local segmental motions, chains mobility, and finally, an increment in water absorption capacity of the sample. Also, AV has a high water absorption capacity, so the addition of this material to the CS/PVA hydrogel could increase the hydrophilic property of the sample. Furthermore, based on the SEM analysis (Fig. 5b), the porosity of the hydrogels increases by the addition of 5 wt.% AV resulted in the swelling capacity enhancement [44]. Swelling ratio is reduced by adding 0.5, 1, and 2 wt.% ZnO-NPs content to the CS/PVA/AV hydrogel. The decrease in the swelling capacity of nanocomposite hydrogels may be related to the decrease in porosity of hydrogels as seen in SEM images (Fig. 5).

As it was previously mentioned, the hydrogel porosity was decreased by the addition of ZnO-NPs, leading to a reduction in water absorption capacity and swelling of the hydrogel. As seen in Fig. 6a, the hydrogel with 2 wt.% content of ZnO-NPs shows a greater swelling ratio than those of with 0.5 and 1 wt.% ZnO-NPs. This indicates that the presence of a proper amount of ZnO nanoparticles may increase the free volume of the polymer blend in the hydrogel network, which in turn facilitates the penetration of water into the hydrogel [53]. The SEM images (Fig. 5) confirm the obtained results of swelling ratio.

Weight loss analysis

Biodegradation of wound dressing films is important during wound healing and should be commensurate with the skin regeneration process. Unlike conventional wound dressings, such as bandages, gauze, or cotton wool, modern hydrogels require a moist wound environment which can prevent cell death and accelerate the healing process. These hydrogels dissolve to some extent in contact with wound fluid, and this process results in the formation of a soluble hydrophilic gel that protects the wound and stimulates granulation and epithelialization [53, 54]. Figure 6b shows the weight loss curves of CS/PVA, CS/PVA/AV, and CS/PVA/AV/ZnO nanocomposite hydrogels during 7 days of incubation in PBS at 37° C. All films showed rapid weight loss on the first day. Adding the AV to the hydrogel structure accelerated weight loss compared to the CS/PVA hydrogel. The hydrophilic nature of AV and disturbing the CS/PVA polymer network by the addition of AV are two main reasons causing CS/PVA/AV shows a higher degradation rate (weight loss) than that of CS/PVA hydrogel. As seen in Fig. 6b, the addition of 5 wt.% ZnO-NPs to CS/PVA/AV hydrogel leads to an increase in weight loss percent. Increasing the ZnO-NPs content results in the reduction of weight loss value, whereas the hydrogel with 2 wt.% ZnO-NPs shows a less degradation rate than other hydrogels.

Porosity

Porosity measurements showed that the prepared hydrogels have the porosity in the range of 74–86% (Fig. 6b). The highly porous nature of the bandage is useful for absorbing large volumes of wound discharge from the wound surface. In addition, the porous nature of the bandage increases the distribution of nutrients for the cells attached to it. The results reveal that the nanocomposite hydrogel with 2% nanoparticles has the highest percent of porosity (86%). Previous research has shown that

the presence of a reasonable amount of ZnO nanoparticles may increase the free space in the hydrogel network, which in turn facilitates the expansion and penetration of water [55].

Water vapor transmission rate (WVTR)

Keeping the wound's surface moist is an essential requirement for an ideal wound dressing. The potential of hydrogel dressings is expressed in the transfer of body fluids or wound exudates with the rate of water vapor transfer, directly regulating ambient humidity for proper wound healing. Reduction of the WVTR leads to the accumulation of wound exudate and infection, delays the healing process, and increases the risk of bacterial growth. On the other hand, a higher value of WVTR facilitates faster drying and leads to more scar formation. Therefore, a controlled moisture balance is necessary for optimal wound healing [56]. Figure 6d shows the WVTR of the prepared hydrogels over 24 h. As can be seen, the WVTR increases by 68.98% with the addition of 5 wt.% content of *Aloe vera* to CS/PVA hydrogel. The significant increase in WVTR may be due to the greater porosity of the CS/PVA/AV compared to the CS/PVA hydrogel, as depicted in the SEM images and the swelling results. It is obvious that the high porosity of the hydrogel facilitates the penetration and transfer of water vapor through it. Furthermore, according to the previous studies [57], *Aloe vera* has shown great water absorption ability and a proper water transport tendency, so the addition of 5 wt.% AV to the CS/PVA hydrogel increases the WVTR remarkably. As seen in Fig. 6d, the addition of 0.5 wt.% content of ZnO-NPs to CS/PVA/AV hydrogel decreases the rate of water vapor transmission by 50.9%. Further addition in ZnO-NPs content from 0.5 to 2 wt.% increases the value of WVTR from 2605 to 4669, respectively.

According to the SEM analysis and the porosity measurement of hydrogels, the porosity increases with increase in the ZnO-NPs content in nanocomposite hydrogels. Thus, due to the existence of the free volume and pores in the hydrogel matrix, water vapor could penetrate easily through the hydrogel membrane, so the value of WVTR increases by increasing the porosity.

Investigation of skin absorption

Figure 7a shows the preparation steps of rat skin to perform the skin absorption test. The results of UV–Vis analysis on the solution of release (pH = 7.4) medium in different time intervals for nanocomposite hydrogels incorporating ZnO-NPs are shown in Fig. 7b. As seen, the nanocomposite hydrogel with 0.5wt.% ZnO-NPs shows the highest skin absorption in the early hours compared to other nanocomposite hydrogels (with 1 and 2 wt.% ZnO-NPs). This observation is may be due to the greater degradation rate of CS/PVA/AV/ZnO-NPs(0.5%) nanocomposite hydrogel than the other ones, seen in Fig. 6b. It is concluded that the release of ZnO-NPs from the hydrogel containing a higher percentage of ZnO-NPs is slower in the first 24 h than the hydrogel with a lower percentage of ZnO-NP. However, after 48 h, the release of the hydrogel containing 0.5% ZnO-NPs is fixed, while the hydrogels with 1 and 2 ZnO-NPs have an upward release percentage.

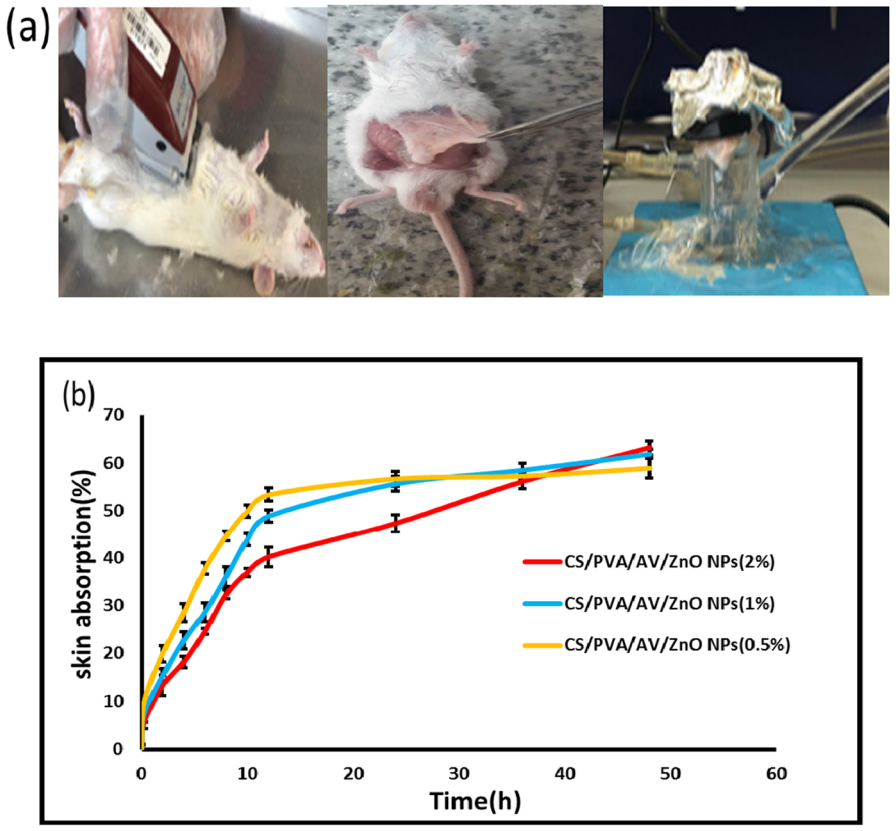

Fig. 7 **a** Skin preparation steps, **b** dermal absorption of zinc nanoparticles from nanocomposite hydrogels

In vitro cell viability analysis

The cytotoxicity of nanocomposite hydrogels was evaluated using MTT assay. Cell metabolic activity is measured using this method, which can be related to the number of living cells. In the current work, the interaction of fibroblast cells with the prepared hydrogels after 48 h of incubation in cell culture medium at 37° C was investigated. For the hydrogel samples, these values are above 90% which are above the toxicity limit (Fig. 8). Thus, the biocompatibility results demonstrate that the nanocomposite dressing hydrogels (CS/PVA/AV/ZnO) do not have cytotoxic properties. This observation confirms the potential application of prepared hydrogels as wound dressings. Sathiyaseelan et al. [58] investigated the cytotoxic properties of chitosan composites incorporating *Aloe vera* and silver nanoparticles. They concluded that the addition of *Aloe vera* to chitosan not only did not cause any cytotoxic properties, but also significantly increased cell viability compared to the composites which are free from *Aloe vera* [58]. Cell viability of PVA/Chitosan/ZnO nanocomposite

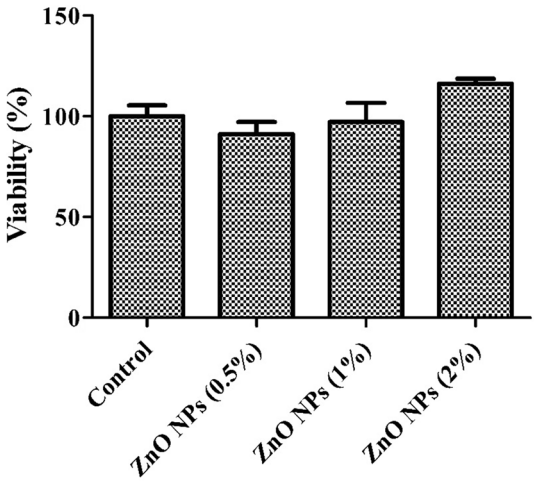

Fig. 8 Cell viability histogram based on MTT assay for nanocomposite hydrogels compared to control group (CS/PVA/AV)

hydrogels was investigated [57]. They reported that the reaction between ZnO-NPs and cells reduced cell survival within 24 h, and then the growth and proliferation of surviving cells increased after 24 h.

Antibacterial activity of hydrogels

The antibacterial activity of prepared hydrogels was evaluated using *Escherichia coli* and *Staphylococcus aureus* by disk diffusion method. The antibacterial mechanism of ZnO-NPs occurs through the release of Zn^{+2} ions and the degradation of proteins and lipids in the bacterial cell wall membrane [23]. Similar mechanisms have been proposed for the antibacterial mechanism of chitosan. The NH_3^+ ions in the chitosan structure can interact with negative ions of cell membranes, leading to cytoplasm leakage into the extracellular matrix. In addition, chitosan shows a higher antibacterial activity at lower PH, which is proper for wound healing because the wound medium is acidic [12].

Photographs of the inhibition zone of the different prepared hydrogels against *S. aureus* and *E. coli* in disk diffusion test are shown in Fig. 9a, b. As seen in Fig. 9a, b, all samples showed bacterial growth inhibitory halo against both bacterial strains due to the presence of antibacterial materials of CS and ZnO-NPs in the structure of hydrogels. The addition of 0.5 wt.% ZnO-NPs causes an increase in the antibacterial activity of hydrogel where the CS/PVA/AV/ZnO(0.5%) shows the highest inhibition zone against *E. coli*. Considering that the nanocomposite hydrogel with 0.5% by weight of ZnO-NPs had more release in 24 h than the nanocomposite hydrogels with 1 and 2% by weight of ZnO-NPs, and while after 48 h, the release of the hydrogel containing 0.5% of ZnO-NPs is fixed, and the hydrogels with 1 and 2% ZnO-NPs have higher release percentages. It can be concluded that for the antibacterial test of hydrogels in 24 h, it seems logical that the antibacterial activity is lower for higher percentages that have a better release after 48 h.

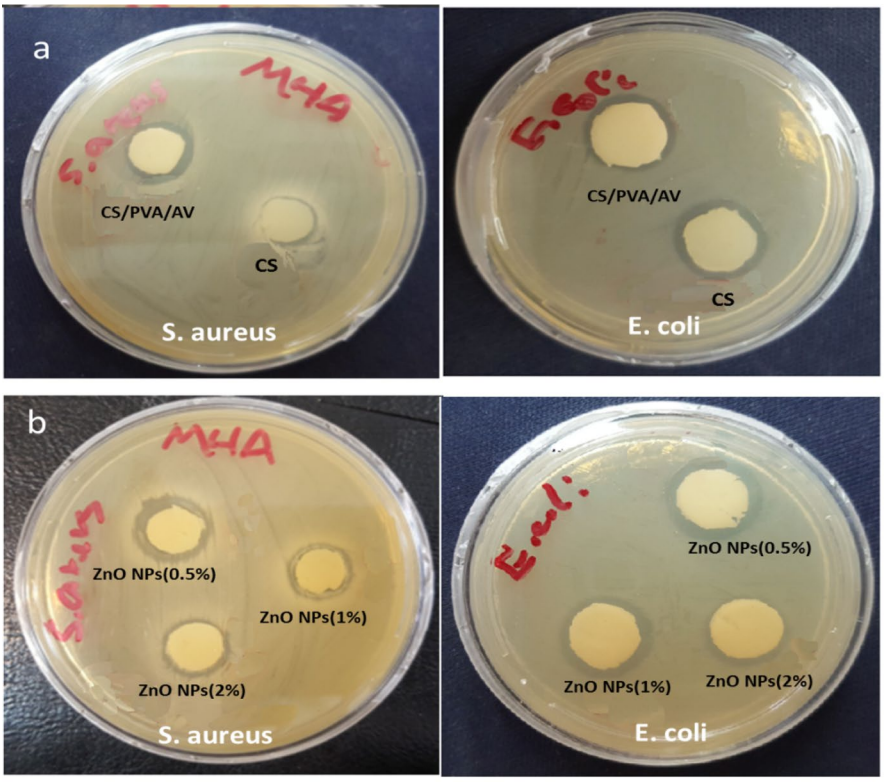

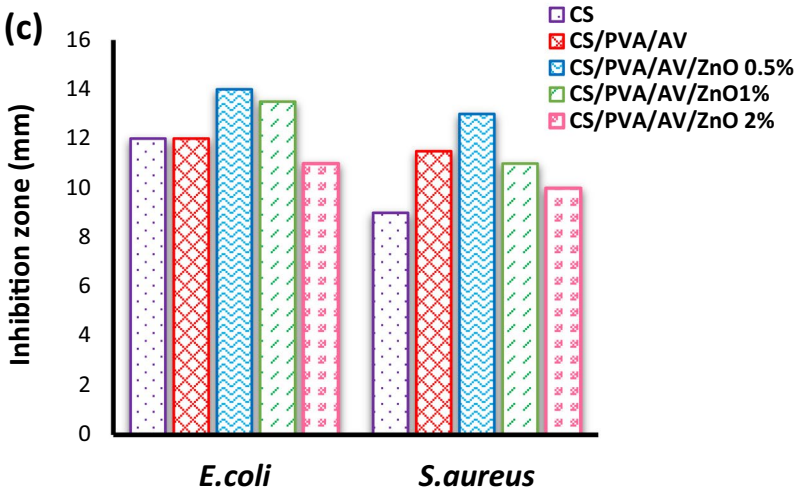

Fig. 9 Antibacterial activity of prepared hydrogels: **a** CS and CS/PVA/AV hydrogels, **b** nanocomposite hydrogels containing ZnO-NPs, and **c** inhibition zones (mm) within 24 h against *S. aureus* and *E. coli*

Conclusions

In this study, hydrogels based on CS/PVA blend incorporating *Aloe vera* and nanoparticles of zinc oxide were prepared for the first time as wound dressings. ZnO-NPs were successfully synthesized using *Matricaria chamomilla* extract. The FE-SEM images and XRD analysis confirmed the nanoscale size of the obtained ZnO nanoparticles. Among the CS/PVA/AV hydrogels with different content *of Aloe vera* (5, 10, and 15%), the hydrogel containing 5 wt.% *Aloe vera* was selected to incorporate the ZnO-NPs due to its higher flexibility. The results showed that the addition of 5 wt.% *Aloe vera* to the CS/PVA hydrogel had a significant effect on increasing the porosity, swelling ratio, degradation rate, WVTR, and mechanical properties. It is concluded that by increasing the content of nanoparticles, the porosity, WVTR, swelling ratio, tensile strength, Young's modulus, and elongation at break increased while the degradation rate decreased. The dermal adsorption studies showed a controlled release of ZnO-NPs from nanocomposite hydrogels. Cell viability studies also proved no cytotoxicity in nanocomposite hydrogels even at high nanoparticle concentrations. The antibacterial activity of the samples demonstrated that the CS/PVA/AV/ZnO (0.5%) hydrogel had a higher antibacterial activity than the other nanocomposite hydrogels. The results showed that based on the type of the wound and timing of its administration, the prepared hydrogels have an excellent potential for use as a wound dressing. The wound healing process on live rat skin was not investigated in this study, but it can be done in future works.

Acknowledgements The authors gratefully acknowledge the research council of Kermanshah University of Medical Sciences (990995) for financial support.

Data availability The data used to support the findings of this study are included within the article.

Declarations

Conflict of interest The authors declare no conflict of interest in the article.

References

1. Böttcher-Haberzeth S, Biedermann T, Reichmann E (2010) Tissue engineering of skin. Burns 36(4):450–460
2. Hanna JR, Giacopelli JA (1997) A review of wound healing and wound dressing products. J Foot Ankle Surg 36(1):2–14
3. Boateng JS et al (2008) Wound healing dressings and drug delivery systems: a review. J Pharm Sci 97(8):2892–2923
4. Singh TRR, Laverty G, Donnelly R (2018) Hydrogels: design, synthesis and application in drug delivery and regenerative medicine. CRC Press, Boca Raton
5. Utech S, Boccaccini AR (2016) A review of hydrogel-based composites for biomedical applications: enhancement of hydrogel properties by addition of rigid inorganic fillers. J Mater Sci 51(1):271–310
6. Petersen DK, Naylor TM, Halen JPV (2014) Current and future applications of nanotechnology in plastic and reconstructive surgery. Plast Aesthet Res 1:43–50
7. Kamoun EA, Kenawy E-RS, Chen X (2017) A review on polymeric hydrogel membranes for wound dressing applications: PVA-based hydrogel dressings. J Adv Res 8(3):217–233

8. Depan D et al (2011) Structure–process–property relationship of the polar graphene oxide-mediated cellular response and stimulated growth of osteoblasts on hybrid chitosan network structure nanocomposite scaffolds. Acta Biomater 7(9):3432–3445
9. Liu X et al (2011) Chitosan-based biomaterials for tissue repair and regeneration. Chitosan Biomater II:81–127
10. Sotelo-Boyás M et al (2017) Physicochemical characterization of chitosan nanoparticles and nanocapsules incorporated with lime essential oil and their antibacterial activity against food-borne pathogens. LWT 77:15–20
11. Hassiba AJ et al (2016) Review of recent research on biomedical applications of electrospun polymer nanofibers for improved wound healing. Nanomed J 11(6):715–737
12. Gutha Y et al (2017) Antibacterial and wound healing properties of chitosan/poly (vinyl alcohol)/zinc oxide beads (CS/PVA/ZnO). Int J Biol Macromol 103:234–241
13. Song T, Tanpichai S, Oksman K (2016) Cross-linked polyvinyl alcohol (PVA) foams reinforced with cellulose nanocrystals (CNCs). Cellulose 23(3):1925–1938
14. Feiz S, Navarchian AH (2019) Poly (vinyl alcohol) hydrogel/chitosan-modified clay nanocomposites for wound dressing application and controlled drug release. Macromol Res 27(3):290–300
15. Bialik-WĄs K et al (2012) The effect of dispersant concentration on properties of bioceramic particles. Dig J Nanomater Biostruct 7(1):361–366
16. Guzmán-Gómez O et al (2018) Amelioration of ethanol-induced gastric ulcers in rats pretreated with phycobiliproteins of Arthrospira (Spirulina) Maxima. Nutrients 10(6):763
17. Majumder R, Das CK, Mandal M (2019) Lead bioactive compounds of *Aloe vera* as potential anticancer agent. Pharmacol Res 148:104416
18. Moon E-J et al (1999) A ncovel angiogenic factor derived from *Aloe vera* gel: β-sitosterol, a plant sterol. Angiogenesis 3(2):117–123
19. Singh B et al (2012) Design of *Aloe vera*-alginate gastroretentive drug delivery system to improve the pharmacotherapy. Polym Plast Technol Eng 51(13):1303–1314
20. Rezaei B, Lotfi-Forushani H, Ensafi A (2014) Modified Au nanoparticles-imprinted sol–gel, multiwall carbon nanotubes pencil graphite electrode used as a sensor for ranitidine determination. Mater Sci Eng C 37:113–119
21. Hu M et al (2018) Zinc oxide/silver bimetallic nanoencapsulated in PVP/PCL nanofibres for improved antibacterial activity. Artif Cells Nanomed Biotechnol 46(6):1248–1257
22. Liu Y-J et al (2009) Antibacterial activities of zinc oxide nanoparticles against Escherichia coli O157: H7. J Appl Microbiol 107(4):1193–1201
23. Khorasani MT et al (2018) Incorporation of ZnO nanoparticles into heparinised polyvinyl alcohol/chitosan hydrogels for wound dressing application. Int J Biol Macromol 114:1203–1215
24. Zhang X et al (2019) Hydrothermal synthesis of Ag nanoparticles on the nanocellulose and their antibacterial study. Inorg Chem Commun 100:44–50
25. Cai Y et al (2017) Large-scale and facile synthesis of silver nanoparticles via a microwave method for a conductive pen. RSC Adv 7(54):34041–34048
26. Francesko A et al (2017) Sonochemical synthesis and stabilization of concentrated antimicrobial silver-chitosan nanoparticle dispersions. Appl Polym Sci 134(30):45136
27. Gupta S, Prakash R (2014) Photochemically assisted formation of silver nanoparticles by dithizone, and its application in amperometric sensing of cefotaxime. J Mater Chem C 2(33):6859–6866
28. Dhayagude AC et al (2018) γ-Radiation induced synthesis of silver nanoparticles in aqueous poly (N-vinylpyrrolidone) solution. Colloids Surf A Physicochem Eng Asp 556:148–156
29. Ahmad N et al (2010) A kinetic study of silver nanoparticles formation from paracetamol and silver (I) in aqueous and micellar media. Colloids Surf B 78(1):109–114
30. Al-Thabaiti NS, Malik MA, Khan Z (2017) Protein interactions with silver nanoparticles: green synthesis, and biophysical approach. Int J Biol Macromol 95:421–428
31. Siddiquee MA et al (2020) Green synthesis of silver nanoparticles from *Delonix regia* leaf extracts: in-vitro cytotoxicity and interaction studies with bovine serum albumin. Mater Chem Phys 242:122493
32. Ogunyemi SO et al (2019) Biosynthesis and characterization of magnesium oxide and manganese dioxide nanoparticles using *Matricaria chamomilla* L. extract and its inhibitory effect on *Acidovorax oryzae* strain RS-2. Artif Cells Nanomed Biotechnol 47(1):2230–2239
33. Hajian M, Mahmoodi M, Imani R (2017) In vitro assessment of poly (vinyl alcohol) film incorporating *Aloe vera* for potential application as a wound dressing. J Macromol Sci 56(7):435–450
34. Batool S et al (2019) Biogenic synthesis of silver nanoparticles and evaluation of physical and antimicrobial properties of Ag/PVA/starch nanocomposites hydrogel membranes for wound dressing application. J Drug Deliv Sci Technol 52:403–414

35. Samadian H et al (2019) Sciatic nerve regeneration by using collagen type I hydrogel containing naringin. J Mater Sci 30(9):1–12
36. Ehterami A et al (2020) A promising wound dressing based on alginate hydrogels containing vitamin D3 cross-linked by calcium carbonate/d-glucono-δ-lactone. Biomed Eng Lett 10(2):309
37. Kokabi M, Sirousazar M, Hassan ZM (2007) PVA–clay nanocomposite hydrogels for wound dressing. Eur Polym J 43(3):773–781
38. Rambabu K et al (2021) Green synthesis of zinc oxide nanoparticles using *Phoenix dactylifera* waste as bioreductant for effective dye degradation and antibacterial performance in wastewater treatment. J Hazard Mater 402:123560
39. Batool M et al (2021) Adsorption, antimicrobial and wound healing activities of biosynthesised zinc oxide nanoparticles. Chem Pap 75(3):893–907
40. Awwad AM et al (2020) Green synthesis of zinc oxide nanoparticles (ZnO-NPs) using *Ailanthus altissima* fruit extracts and antibacterial activity. Chem Int 6(3):151–159
41. Raafat AI et al (2018) Radiation fabrication of Xanthan-based wound dressing hydrogels embedded ZnO nanoparticles: In vitro evaluation. Int J Biol Macromol 118:1892–1902
42. Wang Z et al (2002) Low-temperature synthesis of ZnO nanoparticles by solid-state pyrolytic reaction. Nanotechnology 14(1):11
43. Sagar Raut D, Thorat R (2015) Green synthesis of zinc oxide (ZnO) nanoparticles using *Ocimum tenuiflorum* leaves. Int J Sci Res Publ 4(5):1225–1228
44. Bialik-Wąs K et al (2021) Advanced SA/PVA-based hydrogel matrices with prolonged release of *Aloe vera* as promising wound dressings. Mater Sci Eng C 120:111667
45. Jithendra P et al (2013) Preparation and characterization of *Aloe vera* blended collagen-chitosan composite scaffold for tissue engineering applications. ACS Appl Mater Interfaces 5(15):7291–7298
46. Cui L et al (2014) Preparation and characterization of IPN hydrogels composed of chitosan and gelatin cross-linked by genipin. Carbohydr Polym 99:31–38
47. Escobar-Sierra DM, Perea-Mesa YP (2017) Manufacturing and evaluation of Chitosan, PVA and *Aloe vera* hydrogels for skin applications. Dyna 84(203):134–142
48. Jayakumar R et al (2011) Biomaterials based on chitin and chitosan in wound dressing applications. Biotechnol Adv 29(3):322–337
49. Bonilla J et al (2014) Physical, structural and antimicrobial properties of poly vinyl alcohol–chitosan biodegradable films. Food Hydrocoll. 35:463–470
50. AbdElhady M (2012) Preparation and characterization of chitosan/zinc oxide nanoparticles for imparting antimicrobial and UV protection to cotton fabric. Int J Carbohydr Chem. https://doi.org/10.1155/2012/840591
51. Drabczyk A et al (2020) Physicochemical investigations of chitosan-based hydrogels containing *Aloe vera* designed for biomedical use. Materials 13(14):3073
52. Baghaie S et al (2017) Wound healing properties of PVA/starch/chitosan hydrogel membranes with nano zinc oxide as antibacterial wound dressing material. J Biomater Sci Polym Ed 28(18):2220–2241
53. Yadollahi M et al (2016) Facile synthesis of chitosan/ZnO bio-nanocomposite hydrogel beads as drug delivery systems. Int J Biol Macromol 82:273–278
54. Guo S, DiPietro LA (2010) Factors affecting wound healing. J Dent Res 89(3):219–229
55. Pereira R, Mendes A, Bártolo P (2013) Alginate/*Aloe vera* hydrogel films for biomedical applications. Procedia CIRP 5:210–215
56. Xu R et al (2016) Controlled water vapor transmission rate promotes wound-healing via wound re-epithelialization and contraction enhancement. Sci Rep 6(1):1–12
57. Pereira RF et al (2013) Influence of *Aloe vera* on water absorption and enzymatic in vitro degradation of alginate hydrogel films. Carbohydr Polym 98(1):311–320
58. Sathiyaseelan A et al (2017) Fungal chitosan based nanocomposites sponges—an alternative medicine for wound dressing. Int J Biol Macromol 104:1905–1915

Authors and Affiliations

Hosna Alvandi[1] · Hajar Rajati[1] · Tahereh Naseriyeh[1] · Seyyed Soheil Rahmatabadi[2] · Leila Hosseinzadeh[3] · Elham Arkan[1]

✉ Elham Arkan
elhamarkan@yahoo.com; e.arkan@kums.ac.ir

[1] Nano Drug Delivery Research Center, Health Technology Institute, Kermanshah University of Medical Sciences, Kermanshah 6734667149, Iran

[2] Medical Biology Research Center, Health Technology Institute, Kermanshah University of Medical Sciences, Kermanshah, Iran

[3] Pharmaceutical Sciences Research Center, Health Technology Institute, Kermanshah University of Medical Sciences, Kermanshah 6734667149, Iran